THE JOURNAL OF PHYSICAL CHEMISTRY Letters

Letter

Cite This: J. Phys. Chem. Lett. 2019, 10, 911−917

pubs.acs.org/JPCL

Europium Cyclooctatetraene Nanowire Carpets: A Low-Dimensional, Organometallic, and Ferromagnetic Insulator

Felix Huttmann,[†] Nico Rothenbach,[‡] Stefan Kraus,[†] Katharina Ollefs,[‡] Lucas M. Arruda,[§] Matthias Bernien,[§] Danny Thonig,[∥] Anna Delin,[∥,⊥,#] Jonas Fransson,[∥] Kurt Kummer,[▽] Nicholas B. Brookes,[▽] Olle Eriksson,[∥,○] Wolfgang Kuch,[§] Thomas Michely,[†] and Heiko Wende*[,‡]

[†]II. Physikalisches Institut, Universität zu Köln, Zülpicher Strasse 77, D-50937 Köln, Germany

[‡]Fakultät für Physik, Universität Duisburg-Essen and Center for Nanointegration Duisburg-Essen (CENIDE), Lotharstr. 1, D-47057 Duisburg, Germany

[§]Institut für Experimentalphysik, Freie Universität Berlin, Arnimallee 14, 14195 Berlin, Germany

[∥]Department of Physics and Astronomy, Materials Theory, Uppsala University, SE-75120 Uppsala, Sweden

[⊥]Department of Applied Physics, School of Engineering Sciences, KTH Royal Institute of Technology, Electrum 229, SE-16440 Kista, Sweden

[#]SeRC (Swedish e-Science Research Center), KTH Royal Institute of Technology, SE-10044 Stockholm, Sweden

[▽]European Synchrotron Radiation Facility, 71 Avenue des Martyrs, CS40220, F-38043 Grenoble, Cedex 9, France

[○]School of Science and Technology, Örebro University, SE-701 82 Örebro, Sweden

Supporting Information

ABSTRACT: We investigate the magnetic and electronic properties of europium cyclooctatetraene (EuCot) nanowires by means of low-temperature X-ray magnetic circular dichroism (XMCD) and scanning tunneling microscopy (STM) and spectroscopy (STS). The EuCot nanowires are prepared in situ on a graphene surface. STS measurements identify EuCot as an insulator with a minority band gap of 2.3 eV. By means of Eu $M_{5,4}$ edge XMCD, orbital and spin magnetic moments of $(-0.1 \pm 0.3)\mu_B$ and $(+7.0 \pm 0.6)\mu_B$, respectively, were determined. Field-dependent measurements of the XMCD signal at the Eu M_5 edge show hysteresis for grazing X-ray incidence at 5 K, thus confirming EuCot as a ferromagnetic material. Our density functional theory calculations reproduce the experimentally observed minority band gap. Modeling the experimental results theoretically, we find that the effective interatomic exchange interaction between Eu atoms is on the order of millielectronvolts, that magnetocrystalline anisotropy energy is roughly half as big, and that dipolar energy is approximately ten times lower.

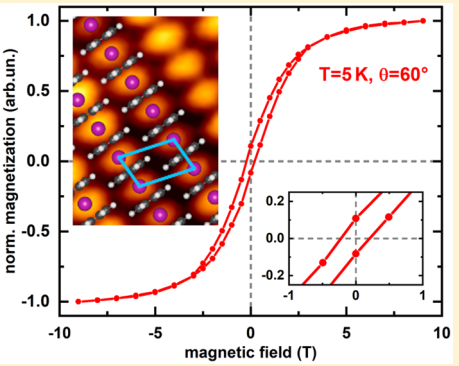

Sandwich molecular wires (SMWs) are a particular 1D class of organometallic structures, distinct from 0D molecular magnets,[1,2] 2D organometallic networks,[3−5] and molecular magnetic hybrid structures on surfaces.[6,7] They consist of a periodic sequence of 4f rare-earth metal cations, predominantly ionically bound and eight-fold coordinated to planar aromatic anions, based on the cyclooctatetraene (C_8H_8 (Cot)) molecule as a ligand.[8] Because of organometallic hybridization between the metal atomic states and the extended π orbitals of the Cot, the metal ions in the wire were proposed to couple magnetically.[9] These systems could be more stable magnetic units than single-molecule magnets and could display larger magnetic anisotropy with correspondingly higher blocking temperatures.

A prime example is the europium cyclooctatetraene (EuCot) SMW, for which chain lengths of up to 30 formula units could be achieved by Hosoya et al. through gas-phase synthesis.[10] Liquid-phase synthesis was realized by Tsuji et al.,[11] although the product was contaminated with ferromagnetic EuO, making the interpretation of its magnetic properties problematic. Recently, some of us introduced an on-surface synthesis method for EuCot, which operates under ultra-high-vacuum conditions and yields a clean, phase-pure product with wire lengths up to 1000 formula units.[12]

In Stern−Gerlach-type experiments by Miyajima et al.,[13] the magnetic moment of EuCot was found to increase linearly with chain length and to be consistent with $m = 7\mu_B$ for each Eu ion, as expected for Eu^{2+}. Although experiments up to now could not make a statement on the presence of magnetic coupling between the paramagnetic Eu^{2+} ions in EuCot, in density

Received: December 12, 2018
Accepted: February 4, 2019
Published: February 4, 2019

DOI: 10.1021/acs.jpclett.8b03711
J. Phys. Chem. Lett. 2019, 10, 911−917

functional theory (DFT) calculations, a ferromagnetic coupling of the Eu^{2+} ions with $m = 7\mu_B$ is invariably found.[9,14−16] For the infinite wire, the ferromagnetic state is favored over the antiferromagnetic state by 2.5 meV according to Atodiresei et al.,[9] by 6 meV in the calculations of Xu et al.,[15] and by 1.2 meV in theoretical work of Yao et al.[16] EuCot is semiconducting, with electronic band gaps of 2.0 and 1.92 eV for the majority channel and of 3.1 and 2.94 eV for the minority channel, as found in the DFT calculations of Xu et al.[15] and Yao et al.,[16] respectively. Furthermore, EuCot wires suspended between Au electrodes were proposed to be nearly perfect spin filters by Xu et al.[15]

On the basis of the new on-surface synthesis method for EuCot, in this contribution, we investigate the magnetic and electronic properties of EuCot SMWs experimentally by using element-specific low-temperature X-ray magnetic circular dichroism (XMCD) experiments and scanning tunneling spectroscopy (STS). We experimentally confirm the theoretical proposition of EuCot being a ferromagnetic insulator. At 5 K, we find an open hysteresis loop for magnetization along the wire axis and considerable magnetic anisotropy by angular- and field-dependent XMCD investigations.

Scanning tunneling microscopy (STM), STS, and low-energy electron diffraction (LEED) measurements were conducted in the STM lab in Cologne, whereas X-ray absorption spectroscopy (XAS) and XMCD measurements complemented by sample characterization with STM and microchannel plate (MCP) LEED were conducted at the high-field-magnet end station of the ID32 beamline of the European Synchrotron Radiation Facility (ESRF).

Prior to each experiment, the Ir(111) sample was prepared by cycles of noble-gas sputtering (Xe or Ar) and flash annealing to 1500 (Cologne) or 1670 K (ESRF). At the ESRF, initial oxygen firing at temperatures up to 1670 K was applied, too. A fully closed, well-oriented graphene (Gr) layer was prepared by room-temperature ethylene adsorption until saturation, thermal decomposition at 1470 K, and subsequent high-temperature exposure at 1270 K to 1×10^{-6} mbar ethylene.[17] The same quality Gr sheet was realized at the ESRF through exposure to 1×10^{-6} mbar ethylene for 600 s at a sample temperature of 1500 K. The orientation and closure of the Gr layer were confirmed in both laboratories through LEED and STM. A 60% coverage of Gr/Ir(111) with EuCot nanowire islands of single-layer height was realized by simultaneous room-temperature exposure to a pressure of 5×10^{-7} mbar Cot molecules and a flux of 1.9×10^{16} s^{-1} m^{-2} Eu atoms for 105 s. Cot molecules were admitted through a gas-dosing valve, and Eu was sublimated from a water-cooled Knudsen cell.

The magnetic properties of the Eu ions, in the EuCot nanowires, were investigated by means of XAS and XMCD measurements. The data were taken in drain current mode using fully (100%) circularly polarized light. The magnetic field of up to 9 T was aligned either parallel or antiparallel to the incident X-ray beam. By rotating the sample around the vertical axis, we could adjust the angle, θ, of the incident X-rays to the surface normal between normal incidence ($\theta = 0°$) and grazing incidence ($\theta = 60°$). Hence, we have been able to obtain information about the magnetic anisotropy of the nanowires. The sample can reach temperatures down to ∼5 K and can go up to ∼325 K. To avoid nonmagnetic artifacts due to switching either the magnetic field or the polarization of the X-rays, all magnetic measurements have been done for all four combinations of field direction and polarization. To minimize radiation damage of the EuCot wires, we applied mirror settings that yield a defocusing of 1 mm in the vertical direction, whereas the beam size in the horizontal direction was ∼100 μm. Using these settings, subsequently recorded XAS and field-dependent XMCD magnetization curves did not show significant changes with time. We performed the magnetic measurements on several identically prepared samples to ensure that the total exposition time of our samples to the X-rays was minimized.

The electronic structure calculations employed the full-potential linear muffin-tin RSPt code.[18] The calculations made use of the generalized gradient approximation, and the basis set consisted of spd basis functions, whereas the 4f states were treated as nonhybridizing core states. The 4f shell was allowed to spin-polarize, forming a net spin moment of $7\mu_B$, whereas the orbital moment in accordance with Russell−Saunders coupling was zero. The polarization of the 4f shell also induced a spin-polarization of the itinerant valence electrons via the exchange-correlation functional. The calculations ignored the influence of the substrate and focused only on the free EuCot molecule. Also, the first-principles calculations were performed only for the electronic structure, magnetic moments, and valence stability.

The thermal ground state of atomistic spins $\{\vec{m}_i\} = m_i\{\vec{e}_i\}$ at site i in the Eu wire is obtained from energy minimization by Monte Carlo simulations on the Metropolis algorithm.[19] The Hamiltonian is

$$\mathcal{H} = -\sum_{<i,j>} J\vec{m}_i\cdot\vec{m}_j - \sum_{ij} \vec{m}_i\mathbf{Q}_{ij}\vec{m}_j + K\sum_i (\vec{m}_i\cdot\hat{e})^2 - \mu_B\vec{B}\sum_i \vec{m}_i \quad (1)$$

consisting of a Heisenberg interaction between nearest-neighbor spins of strength J, dipole−dipole interaction via the dipolar tensor, $\mathbf{Q}_{ij}$, in the point-dipole approximation,[20] uniaxial magnetocrystalline anisotropy, and Zeeman term, respectively. K is the anisotropy constant, and $\vec{B}$ is the external magnetic field.

With knowledge about the exchange couplings, J, one can estimate the phase-transition temperature, T_C, from mean field theory via $k_B T_C^{MF} = 3/2\sum_j J_{0j}$ or from Monte Carlo simulations via both the susceptibility, χ, and Binder's fourth cumulant[19] for different simulated system sizes. By definition,[21] the phase-transition temperature, T_C, is determined only from interaction terms in eq 1; K and B are zero. By varying B along the wire, we obtain hysteresis loops, where the coercive field B^{coer} is extracted from an interpolation of the average magnetization as a function of the external magnetic field $M(B)$ and $M(B^{coer}) = 0$. The Monte Carlo simulations were performed using the UppASD software.[22,23]

We simulate a repetition (10 times) of a Eu wire consisting of 1000 atoms without periodic boundary condition to form a carpet. To reduce thermal noise, we account for 15 replicas of this setup. It turned out that this size is still too small to see domain wall nucleation, although it is allowed by the model in eq 1. The easy axis $\vec{e}$ is in-plane and along the wires. J, K, as well as temperature, T, are parameters of our study. Note that the nearest-neighbor interaction, J, is only along the wire; direct exchange between the wires is set to zero.

Figure 1 depicts the structure of the EuCot nanowire film investigated by STS, XAS, and XMCD. As visible in Figure 1a,

DOI: 10.1021/acs.jpclett.8b03711
J. Phys. Chem. Lett. 2019, 10, 911−917

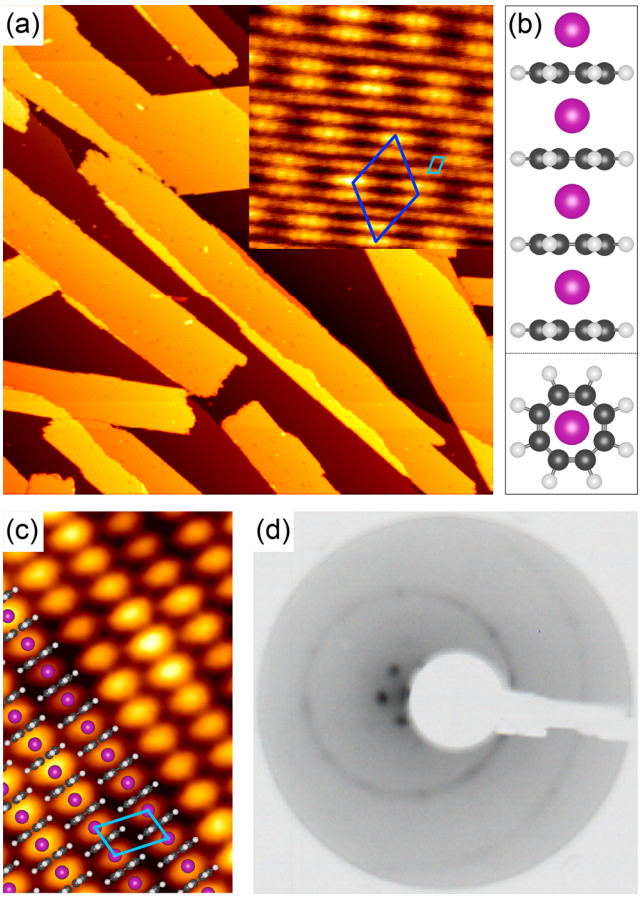

Figure 1. (a) STM topograph of a 0.6 ML EuCot nanowire film on graphene on Ir(111). Image size 260 × 260 nm^2, tunneling voltage U = −3.0 V, tunneling current I = 52 pA. In the inset, the wire structure can be clearly identified. The unit cell of the wire carpet is indicated as a light-blue rhomboid. The hexagonal pattern of height modulations is due to the Gr/Ir(111) moiré. The moiré unit cell is indicated as a dark-blue rhombus and has an edge length of 2.53 nm. Image size 10 × 10 nm^2, U = −3.0 V, I = 58 pA. (b) Side view and view along the wire axis of the DFT-based structure model (Eu, pink; C, dark gray; H, light gray). (c) High-resolution topograph of EuCot, partially overlaid with a structural model and indicating the experimentally measured geometry. The light-blue rhomboid indicates the wire carpet unit cell. Image size 5 × 3 nm^2, U = −3.1 V, I = 60 pA. (d) 42 eV microchannel plate LEED pattern of 0.6 ML EuCot film on Gr/Ir(111) after the film was used for the field-dependent XMCD magnetization curve measurements shown in Figure 3. Two diffraction rings due to EuCot islands and moiré reflections around the (0,0)-spot are present.

the film with a coverage of 0.6 ML is formed. The analysis shows that the islands are (6.1 ± 0.5) Å high with straight edges that consist of parallel nanowires. The islands are distributed in almost random orientation on Gr/Ir(111). Each wire is composed of an alternating sequence of Eu^{2+} cations and Cot^{2-} anions (compare Figure 1b).[10,24] Each Eu^{2+} is eight-fold-coordinated (hapticity η = 8) to neighboring Cot^{2-}. On the basis of STM and LEED, we find primitive translations of the wire carpet unit cell (light blue in the inset of Figure 1a) of 4.4 and 7.15 Å. These values correspond to an intrawire separation of 4.4 Å and an interwire separation of 6.8 Å. The 42 eV MCP-LEED pattern in Figure 1d displays first-order moiré reflections around the (0,0) spot and two concentric diffraction rings characteristic of the EuCot primitive translations defined by the EuCot carpets and consistent with a close-to random orientation distribution of the EuCot islands. A slight preference for island orientations along $\langle 1\bar{1}0\rangle$ and $\langle 11\bar{2}\rangle$ is visible in the MCP-LEED pattern through intensity variations of the diffraction rings. Because of the low electron beam currents, the EuCot MCP-LEED patterns were stable on the time scale of 1000 s and did not show degradation, whereas the EuCot reflections faded away on the time scale of 100 s in standard LEED.

We now turn to the discussion of the XAS and XMCD spectra. Because the magnetism of Eu originates from the 4f electrons, we investigate the Eu $M_{5,4}$ edges, that is, transitions from initial $3d_{5/2}$ and $3d_{3/2}$ to the final 4f states. Figure 2a shows the XAS signal across these edges for a 0.6 ML EuCot coverage on Gr/Ir(111). The measurements were performed at a sample temperature of T = 5 K and an external magnetic field of B = 9 T with left (μ^-) and right (μ^+) circularly polarized X-rays at grazing incidence (θ = 60°) with respect to the sample surface. The spectra are presented on a vertical scale that has been adjusted to zero in the pre-edge region and to one at the peak maximum of the averaged XAS. In these units, a constant value of 1.7 arb.un. corresponding to the pre-edge intensity has been subtracted from all of the spectra.

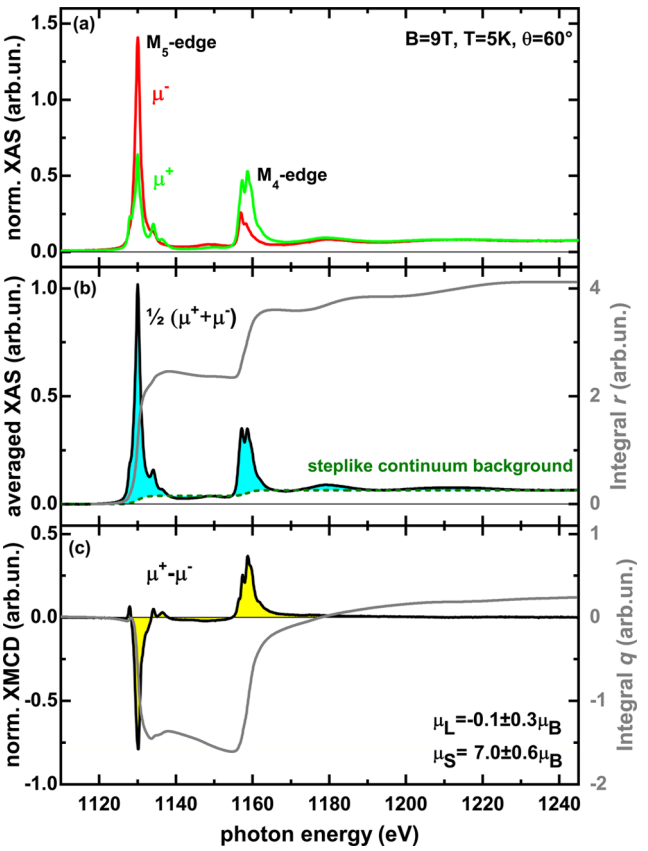

Figure 2. (a) XAS of the Eu M_5 and M_4 edges measured at grazing incidence with θ = 60°, T = 5 K, and B = 9 T, and with left (μ^-) (red solid line) and right (μ^+) (green solid line) circularly polarized X-rays. (b) Polarization-averaged XAS 1/2($\mu^+ + \mu^-$) (black solid line) with a step function (green dashed line) used to separate the $M_{5,4}$ contributions (blue area) from the continuum. Also indicated is the integrated XAS (gray line, right y axis) after background subtraction. (c) Normalized XMCD ($\mu^+ - \mu^-$) (black solid line and yellow area) and integral XMCD (gray line, right y axis).

DOI: 10.1021/acs.jpclett.8b03711
J. Phys. Chem. Lett. 2019, 10, 911−917

Figure 2b shows the polarization-averaged XAS $1/2(\mu^+ + \mu^-)$ with a step-like continuum background. The line shape of the Eu $M_{5,4}$ edge XAS displays clearly divalent Eu^{2+}.[25−27] Therefore, we exclude different integer oxidation states. The 3:2 ratio of the step heights (branching ratio) at the M_5 and M_4 edges results from the degeneracy of the $3d_{5/2}$ and $3d_{3/2}$ orbitals. This is in agreement with Eu XAS analysis in the literature.[27−29] By subtracting the continuum background, we separate the $M_{5,4}$ contributions (blue area) from the averaged XAS. The integral r (Figure 2b, right axis) of the $M_{5,4}$ contributions is used for normalization in the sum-rule analysis.

Figure 2c displays the XMCD signal $(\mu^+ - \mu^-)$ that results from the subtraction of the two absorption spectra with positive and negative helicity. By applying sum-rule analysis to the XMCD data, we can approximate the orbital (μ_L) and spin (μ_S) magnetic moments[28,30]

$$\mu_L = -n_h \frac{q}{r}\mu_B \tag{2}$$

$$\mu_S = -n_h \frac{5p - 3q}{2r}\mu_B - 6\langle T_z\rangle\mu_B \approx -n_h \frac{5p - 3q}{2r}\mu_B \tag{3}$$

where the values p and q (Figure 2c, right axis) describe the integrals of the XMCD over the M_5 and $M_{5,4}$ edges, respectively, n_h identifies the number of holes in the 4f shell (here $n_h = 7$), and r is the integral of the averaged XAS, mentioned above. We approximated the dipolar term $\langle T_z\rangle$ as zero, corresponding to the atomic properties of Eu^{2+} in $4f^7$ configuration.

Applying sum rule analysis, we confirm the orbital moment μ_L to be zero within the error bar of our measurements, that is, $\mu_L = (-0.1 \pm 0.3)\mu_B$, but also allow the interpretation of a small but finite value. For the spin moment, μ_S, we obtain $\mu_S = (+7.0 \pm 0.6)\mu_B$, which is in good agreement with the expectation from the atomic properties of $+7.0\mu_B$. We note: (1) The measured magnetic moments of the Eu ion display, strictly speaking, only the time-averaged projection of the moments along the X-ray direction. We are confident that for a sample temperature of 5 K we are in the vicinity of saturation. Thus we rule out temperature-dependent fluctuations of the calculated magnetic moment and equate them with the true saturated values. (2) Applying the sum rules for rare earths is challenging, in particular due to the uncertainties of the separation of the absorption edges and the long-range magnetic background. For more information on the origin of the errors in the sum rule analysis, see the Supporting Information. In good approximation, the calculated values from the sum rule analysis imply that Eu is present in the half-filled $4f^7$ configuration, as in its bulk state. This is in agreement with the divalent Eu^{2+} state that we derived from the spectral line shape of the averaged XAS.

In addition, we performed XAS and XMCD measurements in a magnetic field of $B = 9$ T for sample temperatures of $T = 7$ and 10 K, which results in a slightly reduced magnetization by 9 and 10%, respectively, as compared with the value at 5 K. This reduction of μ_S is attributed to the ensuing increased spin fluctuations with increasing temperature. For more details of the temperature-dependent XAS measurements, see the Supporting Information.

To investigate the magnetic coupling and anisotropy of the system, in Figure 3, we plot the field-dependent XMCD signal at the M_5 edge normalized to the pre-edge value in dependence on the magnetic field. We assume the Eu magnetization to be proportional to the XMCD signal. The magnetization is given in arbitrary units scaled to a value of 1.0 at $B = 9$ T. Whereas Figure 3a, measured at the lowest attainable temperature of 5 K and normal incidence ($\theta = 0°$), displays no loop opening, Figure 3b, recorded at the same temperature and grazing incidence with $\theta = 60°$, shows a clear hysteresis with a coercive field of 0.2 T (compare the inset of Figure 3b). We note that measuring the in-plane magnetization displays an average of the spectra for the entire EuCot nanowire film, which consists of randomly oriented islands, and therefore is an average of the contributions along the wires and perpendicular to them in the surface plane. Hence, the resulting coercive field is much smaller than the value of 2.5 T, where the magnetization curve closes. After observing an open loop at 5 K, we measured field-dependent XMCD signals at the Eu M_5 edge successively for 10 and 7 K to assess the Curie temperature, T_C, of the EuCot wire carpets. At 10 and 7 K, no open loop is observed. Figure 3c displays exemplarily the 7 K measurement. After cooling to 5 K, the loop reopens again. Hence, the Curie temperature, T_C, lies between 5 and 7 K. These observations are interpreted as clear indications for ferromagnetic coupling of the EuCot nanowire carpet, with the easy magnetization direction in the surface plane.

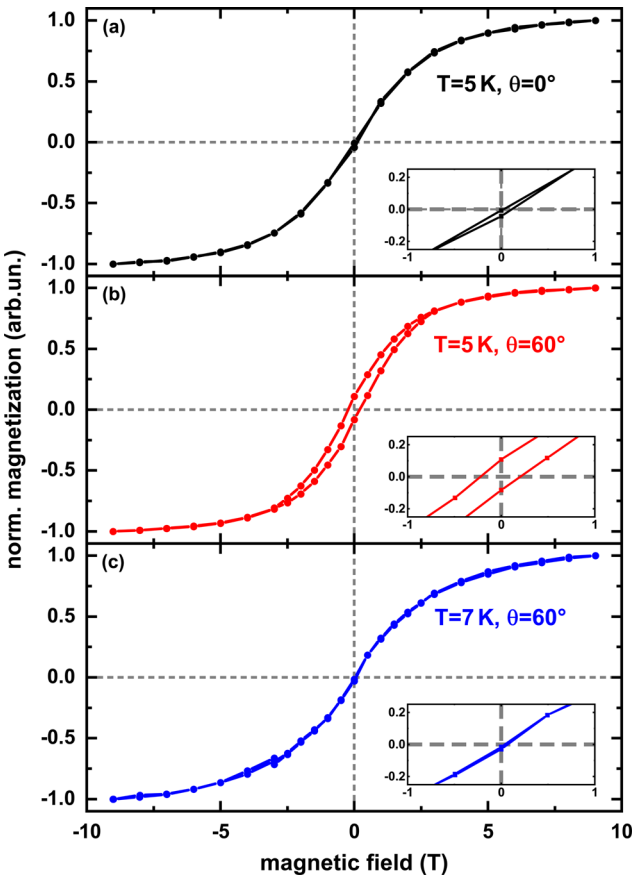

Figure 3. Field-dependent XMCD signal at the Eu M_5 edge (E_{hv} = 1130.1 eV) for $-9\text{ T} \le B \le 9\text{ T}$, normalized such that the field-dependent XMCD signal at $B = 9$ T is 1.0. Insets magnify the magnetization in the range $-1\text{ T} \le B \le 1$ T. (a) Magnetization for normal incidence with $\theta = 0°$ at 5 K. (b) Magnetization for grazing incidence with $\theta = 60°$ at 5 K. (c) Magnetization for grazing incidence with $\theta = 60°$ at 7 K.

DOI: 10.1021/acs.jpclett.8b03711
J. Phys. Chem. Lett. 2019, 10, 911−917

We would like to note that we cannot specify the exact role of graphene on the magnetic anisotropy because we cannot prepare the EuCot wires without the graphene substrate. Hence we cannot perform a similar study like that shown by Lisi et al.,[31] where the anisotropy of the orbital moment of a 2D iron phthalocyanine (FePc) network was compared with a thick FePc film without graphene as a reference. However, such a thick reference film does not exist in our case. Therefore, we cannot identify the influence of graphene on the magnetic anisotropy.

Previous calculations[9] gave the single-ion anisotropy of Eu in EuCot to be on the order of only a few microelectronvolts, consistent with our own DFT calculations. However, as will be discussed below, a much higher magnetocrystalline anisotropy of ∼0.5 meV has to be present to explain the experimental observations. In contrast, the anisotropy energy resulting from the magnetic dipolar interaction is on the order of 100 μeV due to the large moment of 7μ_B and, according to these calculations, would thus entirely dominate the magnetic anisotropy. More precisely, we have calculated the dipolar energy for three different orientations of magnetic moments in the EuCot nanowire carpet: (a) along the wire axis, E_a = −0.0745 meV; (b) perpendicular to wire axis but in the plane of the carpet, E_b = −0.0050 meV; and (c) perpendicular to the plane of the carpet, E_c = +0.0795 meV.

This means that for normal X-ray incidence all wires are magnetized in a hard direction, explaining the absence of hysteresis, whereas for the grazing incidence, despite the random in-plane orientation of the wires, for some EuCot islands a large component of the applied magnetic field is along the easy axis. In this view, the moderate susceptibility at grazing X-ray incidence is tentatively assumed to result from the difficulty to orient the magnetic moments in EuCot wire islands that are substantially misoriented with respect to the projection of the magnetic field onto the sample plane.

We also considered alternative explanations for the magnetization loop opening that can be excluded as explained in the following: (1) One might speculate that ferromagnetic EuO has formed during growth or later by oxidation from the residual gas, which certainly would give rise to a loop opening. However, (i) EuCot synthesis is efficient and performed in large Cot excess, such that we never observed any sign of metallic Eu on the sample with STM after EuCot growth, which also rules out EuO formation during subsequent treatment. Moreover, (ii) EuO is magnetically soft, with a coercive field of <100 mT[32] and thus cannot be responsible for an opening persisting up to 2.5 T. In addition, (iii) EuO has a T_C = 69 K, inconsistent with our finding of $T_C \leq 7$ K for EuCot. (2) We considered that a layer of intercalated Eu under Gr could have accidentally formed, which would be strongly ferromagnetically coupled. However, as already mentioned above, (i) with STM, we never observed any sign of metallic Eu, be it adsorbed or intercalated, on the sample after EuCot growth. Moreover, (ii) intercalated Eu is magnetically soft as well, as discussed in ref 27. The large coercive field can then only be explained by a strong in-plane uniaxial anisotropy, and Eu in EuCot islands is the only possible explanation. Consistent with the magnetic loop opening due to the presence of Eu in EuCot is the fact that the loop opening is subject to X-ray radiation damage when the sample is intentionally illuminated with higher X-ray flux, as typical for an organometallic system. For more details of the effect of radiation damage on the magnetization curves, see the Supporting Information.

Figure 4 provides further insight into the electronic structure of the EuCot nanowires. In Figure 4a, a typical STS point spectrum taken on a monolayer thick EuCot island is provided (see the inset for the location of spectroscopy). From the spectrum, it is obvious that the EuCot wires are insulators. The electronic band gap is estimated to be 2.3 eV and ranges between −0.2 and 2.1 eV. For this estimate, the band edges were identified as the locations where the dI/dV intensity moves just out of the noise level within the gap. Note that because of their localized nature, the Eu 4f states are not expected to contribute to the tunneling current. They are therefore invisible in STM and may be located within the gap as measured by STS. Therefore, the measured band gap corresponds to the minority band gap and is considerably smaller than the ∼3 eV calculated before.[15,16] As the 4f states are occupied and thus located below the Fermi level in the majority channel, the majority band gap is larger than 2.1 eV.

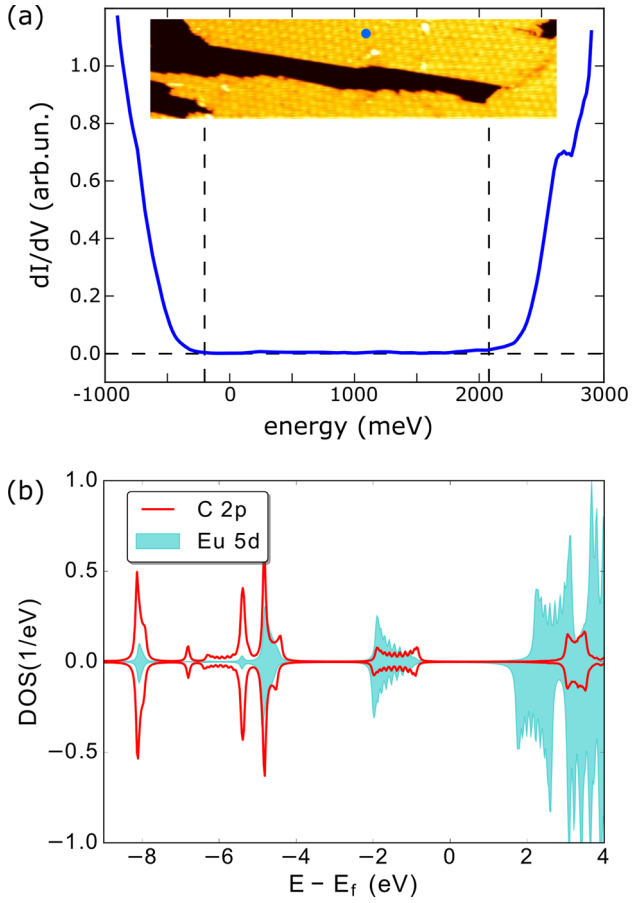

Figure 4. (a) dI/dV point spectrum on a EuCot island. The tip was stabilized at U = −1.0 V and I = 5 nA prior to feedback loop opening. The spectrum displayed is the average over five subsequent spectra, with the same tip at the same location of an EuCot island indicated by the blue dot in the STM topograph shown as an inset. Image size 25 × 100 nm, U = −2.0 V, I = 66 pA. Thin vertical lines indicate positions where the dI/dV signal rises over the noise level in the tunneling gap. (b) Projected density of states for Eu 5d and C 2p orbitals for spin up (positive) and spin down (negative).

The spin components of the density of states (DOS) resulting from our DFT calculations are shown in Figure 4b. As

DOI: 10.1021/acs.jpclett.8b03711
J. Phys. Chem. Lett. 2019, 10, 911−917

can be seen, the system is an insulator with a band gap of ∼2.1 eV, which agrees rather well with the experimentally observed gap. The band gap is determined for our case by the minority channel. In Figure 4b, we show only the dominant parts of the atom and l-projected DOS curves, that is, the C 2p and Eu 5d states. Note that because the 4f electrons are localized, we have excluded them from the graph. However, the 4f electron states may come into play for excitation energies of ∼2 eV because the energy difference between the di- and trivalent state is ∼2 eV. We conclude this based on the Born−Haber analysis presented in the Supporting Information. To be precise, the valences of a bare Eu wire and a EuCot wire are calculated to be divalent, with an energy gap to the trivalent configuration of 1.94 and 2.08 eV, respectively.

Figure 4b shows that there is a significant hybridization between C 2p and Eu 5d states, especially for the occupied states. This shows up most markedly from peaks that have common large intensity of both types of orbitals. The exchange splitting is largest for Eu 5d states, which is most noticeable for the unoccupied states. This exchange splitting is induced by the exchange and correlation from the large spin density of the 4f shell, which has a net moment of $7\mu_B$. The induced exchange splitting of the 5d states is also found for the occupied states, and for this reason a small moment of $0.05\mu_B$ emerges on the Eu valence states (excluding the $7\mu_B$ of the 4f shell). We note here that in this kind of calculation there is also an interstitial contribution to the moment, located between the Eu atom and the Cot molecule, that has an induced magnetization that is difficult to assign to a specific atom or orbital angular momentum state. The net induced moment, summed over interstitial contribution and all atom and angular momentum projected states, is, however, vanishing because the induced moment of $0.05\mu_B$ on Eu states is compensated exactly by the induced interstitial moment and the moment projected on the Cot molecule. This results in a calculated moment of $7\mu_B$/f.u. An integer value of the magnetic moment is a natural outcome of any magnetic insulator because an integer number of bands of the spin-up and spin-down states are occupied.

A theoretical analysis of the dependence of the coercive field with respect to temperature finds that the coercive field decays very fast with respect to temperature and vanishes close to the ordering temperature (compare the Supporting Information). This is in agreement with our observations. The Monte Carlo simulations with an exchange coupling of 1.2 meV matched to the experimental $T_C \approx 6$ K enable us to conclude that in addition to the dipolar anisotropy of ∼0.15 meV an additional and even larger magnetic anisotropy of ∼0.5 meV has to be present to reproduce the experimentally observed coercive field of 0.2 T. Previous[9] DFT calculations yielded magneto-crystalline anisotropies on the order of 5 μeV. We note that the determination of the magnetocrystalline anisotropy energies is very challenging because of the smallness of the values, and we have not attempted to explain the estimated magnetic anisotropy from the DFT calculations. Furthermore, we cannot exclude the presence of other anisotropies in the system, for example, symmetric anisotropy exchange,[33] that are not included in our model or effects stemming from the influence of the substrate.

We have shown experimentally through a combination of XMCD and STS that EuCot is a ferromagnetic insulator. The size of the band gap from the experiment is well reproduced by DFT calculations. We have analyzed the measured results using an effective spin-Hamiltonian that contains interatomic exchange, dipolar energies, magnetic anisotropy, and a Zeeman term. Measurements are reproduced from a model where the interatomic exchange is on the order of millielectronvolts, the magnetic anisotropy is roughly half of the exchange, and dipolar energy is roughly one order of magnitude smaller than the exchange interaction. We are confident that the finding of ferromagnetic ordering in an experimentally well-accessible, surface-supported, organometallic system will provide new inspiration for the field of molecular spintronics.

■ ASSOCIATED CONTENT

Supporting Information

The Supporting Information is available free of charge on the ACS Publications website at DOI: 10.1021/acs.jpclett.8b03711.

Experimental results, including detailed information on the sum-rule analysis, the temperature dependence, and the effect of radiation damage on the absorption spectra and the field-dependent measurements, as well as the theoretical results, including the determination of the valence stability and the finite temperature effects of the coercive field (PDF)

■ AUTHOR INFORMATION

Corresponding Author

*E-mail: heiko.wende@uni-due.de.

ORCID

Felix Huttmann: 0000-0002-8503-7034
Lucas M. Arruda: 0000-0003-3601-9793
Anna Delin: 0000-0001-7788-6127
Jonas Fransson: 0000-0002-9217-2218
Kurt Kummer: 0000-0003-3044-7957
Wolfgang Kuch: 0000-0002-5764-4574
Heiko Wende: 0000-0001-8395-3541

Notes

The authors declare no competing financial interest.

■ ACKNOWLEDGMENTS

We are grateful to Samara Keshavarz for performing the DFT calculations and to Dr. Yaroslav Kvashnin and Nicolae Atodiresei for valuable discussions. We thank the European Synchrotron Radiation Facility (ESRF) for beamtime allocation (experiment HC-2698) and the beamline ID32 staff for the kind support. O.E. acknowledges support from eSSENCE, the Swedish Research Council, the KAW foundation (projects 2013.0020 and 2012.0031), and the Foundation for Strategic Research. H.W. and T.M. acknowledge support from DFG through projects WE 2623/17-1 and MI 581/23-1. H.W. and N.R. acknowledge funding by the Deutsche Forschungsgemeinschaft (DFG, German Research Foundation) - Projektnummer 278162697 - SFB 1242. S.K. and F.H. acknowledge financial support through the Institutional Strategy of the University of Cologne within the German Excellence Initiative. L.M.A., M.B., and W.K. thank the BMBF for financial support (no. 05K13KEA "VEKMAG"). L.M.A. acknowledges CAPES for funding (no. 9469/13-3).

■ REFERENCES

(1) Sanvito, S. Molecular spintronics. *Chem. Soc. Rev.* **2011**, *40*, 3336−3355.

DOI: 10.1021/acs.jpclett.8b03711
J. Phys. Chem. Lett. 2019, 10, 911−917

(2) Cinchetti, M.; Heimer, K.; Wüstenberg, J.-P.; Andreyev, O.; Bauer, M.; Lach, S.; Ziegler, C.; Gao, Y.; Aeschlimann, M. Determination of spin injection and transport in a ferromagnet/organic semiconductor heterojunction by two-photon photoemission. *Nat. Mater.* **2009**, *8*, 115.
(3) Barth, J. Fresh perspectives for surface coordination chemistry. *Surf. Sci.* **2009**, *603*, 1533.
(4) Gambardella, P.; Stepanow, S.; Dmitriev, A.; Honolka, J.; de Groot, F.; Lingenfelder, M.; Gupta, S.; Sarma, D.; Bencok, P.; Stanescu, S.; et al. Supramolecular control of the magnetic anisotropy in two-dimensional high-spin Fe arrays at a metal interface. *Nat. Mater.* **2009**, *8*, 189−193.
(5) Wäckerlin, C.; Nowakowski, J.; Liu, S.; Jaggi, M.; Siewert, D.; Girovsky, J.; Shchyrba, A.; Hählen, T.; Kleibert, A.; Oppeneer, P.; et al. Two-Dimensional Supramolecular Electron Spin Arrays. *Adv. Mater.* **2013**, *25*, 2404−2408.
(6) Wende, H.; Bernien, M.; Luo, J.; Sorg, C.; Ponpandian, N.; Kurde, J.; Miguel, J.; Piantek, M.; Xu, X.; Eckhold, P.; et al. Substrate-induced magnetic ordering and switching of iron porphyrin molecules. *Nat. Mater.* **2007**, *6*, 516.
(7) Bernien, M.; Miguel, J.; Weis, C.; Ali, M.; Kurde, J.; Krumme, B.; Panchmatia, P.; Sanyal, B.; Piantek, M.; Srivastava, P.; et al. Tailoring the Nature of Magnetic Coupling of Fe-Porphyrin Molecules to Ferromagnetic Substrates. *Phys. Rev. Lett.* **2009**, *102*, 047202.
(8) Nakajima, A.; Kaya, K. A Novel Network Structure of Organometallic Clusters in the Gas Phase. *J. Phys. Chem. A* **2000**, *104*, 176−191.
(9) Atodiresei, N.; Dederichs, P. H.; Mokrousov, Y.; Bergqvist, L.; Bihlmayer, G.; Blügel, S. Controlling the Magnetization Direction in Molecules via Their Oxidation State. *Phys. Rev. Lett.* **2008**, *100*, 117207.
(10) Hosoya, N.; Takegami, R.; Suzumura, J.; Yada, K.; Miyajima, K.; Mitsui, M.; Knickelbein, M.; Yabushita, S.; Nakajima, A. Formation and Electronic Structures of Organoeuropium Sandwich Nanowires. *J. Phys. Chem. A* **2014**, *118*, 8298−8308.
(11) Tsuji, T.; Hosoya, N.; Fukazawa, S.; Sugiyama, R.; Iwasa, T.; Tsunoyama, H.; Hamaki, H.; Tokitoh, N.; Nakajima, A. Liquid-Phase Synthesis of Multidecker Organoeuropium Sandwich Complexes and Their Physical Properties. *J. Phys. Chem. C* **2014**, *118*, 5896−5907.
(12) Huttmann, F.; Schleheck, N.; Atodiresei, N.; Michely, T. On-Surface Synthesis of Sandwich Molecular Nanowires on Graphene. *J. Am. Chem. Soc.* **2017**, *139*, 9895−9900.
(13) Miyajima, K.; Yabushita, S.; Knickelbein, M.; Nakajima, A. Stern-Gerlach Experiments of One-Dimensional Metal-Benzene Sandwich Clusters: $M_n(C_6H_6)_m$ (M = Al, Sc, Ti, and V). *J. Am. Chem. Soc.* **2007**, *129*, 8473−8480.
(14) Zhang, X.; Ng, M.-F.; Wang, Y.; Wang, J.; Yang, S.-W. Theoretical Studies on Structural, Magnetic, and Spintronic Characteristics of Sandwiched Eu_nCot_{n+1} (n = 1 − 4) Clusters. *ACS Nano* **2009**, *3*, 2515−2522.
(15) Xu, K.; Huang, J.; Lei, S.; Su, H.; Boey, F.; Li, Q.; Yang, J. Efficient organometallic spin filter based on Europium-cyclooctatetraene wire. *J. Chem. Phys.* **2009**, *131*, 104704.
(16) Yao, X.; Yuan, S.; Wang, J. Theoretical Studies of Sandwich Molecular Wires with Europium and Boratacyclooctatetraene Ligand and the Structure on a H-Ge(001)-2 × 1 Surface. *J. Phys. Chem. C* **2016**, *120*, 7088−7093.
(17) van Gastel, R.; N'Diaye, A.; Wall, D.; Coraux, J.; Busse, C.; Buckanie, N.; Meyer zu Heringdorf, F.-J.; Horn von Hoegen, M.; Michely, T.; Poelsema, B. Selecting a single orientation for millimeter sized graphene sheets. *Appl. Phys. Lett.* **2009**, *95*, 121901.
(18) Wills, J.; Alouani, M.; Andersson, P.; Delin, A.; Eriksson, O.; Grechnev, A. *Full-Potential Electronic Structure Method, Energy and Force Calculations with Density Functional and Dynamical Mean Field Theory*; Springer Series in Solid-State Sciences; Springer-Verlag Berlin Heidelberg, 2010; Vol. *167*.
(19) Binder, K.; Heermann, D. *Monte Carlo Simulation in Statistical Physics: An Introduction*; Springer-Verlag Berlin Heidelberg, 2010; Vol. *5*.
(20) Skubic, B. *Spin Dynamics and Magnetic Multilayers*. Doctoral Dissertation, Uppsala University, 2007.
(21) Nolting, W. *Theoretical Physics 8, Statistical Physics*; Springer International Publishing, 2018.
(22) Uppsala University, Department of Physics and Astronomy. *Uppsala Atomistic Spin Dynamics Code*. http://physics.uu.se/uppasd (accessed 11-6-2018).
(23) Eriksson, O.; Bergman, A.; Bergqvist, L.; Hellsvik, J. *Atomistic Spin Dynamics: Foundations and Applications*; Oxford University Press, 2017.
(24) Kurikawa, T.; Negishi, Y.; Hayakawa, F.; Nagao, S.; Miyajima, K.; Nakajima, A.; Kaya, K. Multiple-Decker Sandwich Complexes of Lanthanide-1,3,5,7-Cyclooctatetraene $[Ln_n(C_8H_8)_m]$ (Ln = Ce, Nd, Eu, Ho, and Yb); Localized Ionic Bonding Structure. *J. Am. Chem. Soc.* **1998**, *120*, 11766−11772.
(25) Thole, B.; van der Laan, G.; Fuggle, J.; Sawatzky, G.; Karnatak, R.; Esteva, J.-M. 3d x-ray-absorption lines and the $3d^9 4f^{n+1}$ multiplets of the lanthanides. *Phys. Rev. B: Condens. Matter Mater. Phys.* **1985**, *32*, 5107.
(26) Förster, D.; Klinkhammer, J.; Busse, C.; Altendorf, S.; Michely, T.; Hu, Z.; Chin, Y.-Y.; Tjeng, L. H.; Coraux, J.; Bourgault, D. Epitaxial europium oxide on Ni(100) with single-crystal quality. *Phys. Rev. B: Condens. Matter Mater. Phys.* **2011**, *83*, 045424.
(27) Schumacher, S.; Huttmann, F.; Petrović, M.; Witt, C.; Förster, D.; Vo-Van, C.; Coraux, J.; Martínez-Galera, A.; Sessi, V.; Vergara, I.; et al. Europium underneath graphene on Ir(111): Intercalation mechanism, magnetism, and band structure. *Phys. Rev. B: Condens. Matter Mater. Phys.* **2014**, *90*, 235437.
(28) Carra, P.; Thole, B.; Altarelli, M.; Wang, X. X-ray circular dichroism and local magnetic fields. *Phys. Rev. Lett.* **1993**, *70*, 694.
(29) Kachkanov, V.; Wallace, M.; van der Laan, G.; Dhesi, S.; Cavill, S.; Fujiwara, Y.; O'Donnell, K. Induced magnetic moment of Eu3+ ions in GaN. *Sci. Rep.* **2012**, *2*, 969.
(30) Thole, B.; Carra, P.; Sette, F.; van der Laan, G. X-ray circular dichroism as a probe of orbital magnetization. *Phys. Rev. Lett.* **1992**, *68*, 1943.
(31) Lisi, S.; Gargiani, P.; Scardamaglia, M.; Brookes, N.; Sessi, V.; Mariani, C.; Betti, M. Graphene-Induced Magnetic Anisotropy of a Two-Dimensional Iron Phthalocyanine Network. *J. Phys. Chem. Lett.* **2015**, *6*, 1690−1695.
(32) Klinkhammer, J.; Förster, D.; Schumacher, S.; Oepen, H.; Michely, T.; Busse, C. Structure and magnetic properties of ultra thin textured EuO films on graphene. *Appl. Phys. Lett.* **2013**, *103*, 131601.
(33) Udvardi, L.; Szunyogh, L.; Palotas, K.; Weinberger, P. First-principles relativistic study of spin waves in thin magnetic films. *Phys. Rev. B: Condens. Matter Mater. Phys.* **2003**, *68*, 104436.

DOI: 10.1021/acs.jpclett.8b03711
J. Phys. Chem. Lett. 2019, 10, 911−917